Validation of Thorpe scale-derived vertical diffusivities against microstructure measurements in the Kerguelen region

Y.-H. Park[1,*], J.-H. Lee[2], I. Durand[1], C.-S. Hong[2]

[1] MNHN-Sorbonne Universités (UPMC, Univ Paris 06)-CNRS-IRD, LOCEAN Laboratory, Muséum National d'Histoire Naturelle, 43, rue Cuvier, F-75005 Paris, France

[2]Korea Institut of Ocean Science & Technology, Ansan, Korea

*Corresponding author: yhpark@mnhn.fr

Tel: (+33) (0)1 4079 3170; Fax: (+33) (0)1 4079 5756

Abstract

The Thorpe scale is an energy containing vertical overturning scale of large eddies associated with shear generated turbulence. This study investigates indirect estimates of vertical diffusivities from the Thorpe scale method in the Polar Front region east of the Kerguelen Islands based on fine scale density profiles gathered during the 2011 KEOPS2 cruise. These diffusivities are validated in comparison with diffusivities estimated from the turbulence dissipation rate directly measured via a TurboMAP microstructure profiler. The results are sensitive to the choice of the diffusivity parameterization and the overturn ratio *Ro*, and the optimal results have been obtained from the parameterization by Shih et al. (2005) and the *Ro* = 0.25 criterion, rather than the parameterization by Osborn (1980) and the *Ro* = 0.2 criterion originally suggested by Gargett and Garner (2008).

The Thorpe scale-derived diffusivities in the KEOPS2 region show a high degree of spatial variability, ranging from a canonical value of $O(10^{-5})$ $m^2 s^{-1}$ in the Winter Water layer and in the area immediately north of the Polar Front to a high value of $O(10^{-4})$ $m^2 s^{-1}$ in the seasonal thermocline between the surface mixed layer and the Winter Water. The latter high diffusivities are found especially over the shallow plateau southeast of the Kerguelen Islands and along the Polar Front that is attached to the escarpment northeast of the islands. The interaction of strong frontal flow with prominent bottom topography likely causes the observed elevated mixing rates.

1. Introduction

Vertical mixing is a dominant factor in controlling vertical fluxes of heat, salt, and nutrients, so the estimation of vertical (or diapycnal) diffusivities especially in the upper layer of the ocean was one of the primary priorities of the physical component of the KEOPS2 cruise. During the cruise, direct turbulence measurements were made at selected stations using a tethered quasi-freefall profiler, TurboMAP, measuring the microstructure of velocity shear. An indirect method

for estimating vertical diffusivities using more accessible CTD (Conductivity-Temperature-Depth) density profiles is the Thorpe scale method (Thorpe, 1977). The objective of this study is to estimate the vertical diffusivities from fine scale density profiles using the Thorpe scale method and validate them in comparison with microstructure measurements collected via a TurboMAP during the KEOPS2 cruise.

The performance of the Thorpe scale method compared to microstructure estimates has been known to depend on the stratification of the water column and surface environment conditions affecting the ship motion. While good agreement between the two methods has been reported in low-latitude regions of high stratification and low winds (Ferron et al., 1998; Klymak et al., 2008), the application of the Thorpe scale method in the Southern Ocean could be compromised because of low stratification and extreme environments (Frants et al., 2013). The latter authors reported that the CTD-based fine structure methods overestimate microstructure diffusivities by one to two orders of magnitude in the southeastern Pacific and Drake Passage, claiming their real limitations in the Southern Ocean.

Another intriguing issue concerns the existence of two different parameterizations of vertical diffusivity K in terms of turbulence dissipation rate ε and buoyancy frequency N. Note that $N^2 = -(g/\rho_0)\rho_z$, where g is gravity, ρ_0 is a constant reference density, and ρ_z is a vertical gradient of potential density calculated at each depth over a vertical extent of 10 m.

For example, Osborn (1980) suggested a well-known parameterization as

$$K = 0.2\varepsilon/N^2. \quad (1)$$

On the other hand, Shih et al. (2005) proposed a new parameterization for the energetic turbulence regime ($\varepsilon/\nu N^2 > 100$) based on the laboratory and numerical experiments as

$$K = 2\nu(\varepsilon/\nu N^2)^{1/2}, \quad (2)$$

where ν = (1.5 to 1.8) x 10^{-6} m^2 s^{-1} is the kinematic viscosity in the temperature range of 0 to 5°C and $\varepsilon/\nu N^2$ is the turbulence intensity parameter. Note that for the moderate turbulence intensity regime ($7 < \varepsilon/\nu N^2 < 100$), the parameterization of K by Shih et al. (2005) is same as (1) proposed by Osborn (1980).

While the TurboMAP measurements lead to direct estimates of ε, the Thorpe scale method gives its indirect estimates by making use of an empirical relationship between the Thorpe scale and ε. These two (direct and indirect) estimates of ε can be applied to the above two parameterizations of K, yielding a total of four kinds of K estimates (Osborn_ε, Osborn_Thorpe, Shih_ε, Shih_Thorpe) at each station of intercomparison. Because of their utmost importance, the detailed procedures for the preliminary processing of CTD data as well as for the detection and validation of overturns for calculating the Thorpe scale are given in section 2. These are largely based on a comprehensive paper by Gargett and Garner (2008), although we have added some modifications. We will show in section 3 that the results are sensitive to the choice of the K parameterization and to the criteria of the overturn validation. In section 4 we present vertical diffusivities in the KEOPS2 area estimated from the optimally chosen parameterization and overturn ratio. Discussion of a displacement shape method recently proposed by van Haren and Gostiaux (2014) is given in section 5, followed by conclusions.

2. Preliminary processing of CTD data

CTD data used for deriving fine scale density profiles were collected during the October-November 2011 KEOPS2 cruise aboard the R/V Marion Dufresne in the Polar Front (PF) region east of the Kerguelen Islands (see Park et al., 2014, for details of the regional hydrography and frontal circulation). Here we used a total of 22 CTD profiles gathered using two sets of Sea-Bird

SBE 9*plus* sensors at stations shown in Fig. 1, where the concomitant TurboMAP stations are shown circled. The CTD profiles mostly extend from the surface to the bottom, while the TurboMAP measurements from the surface to about 400 m, limiting our validation of the Thorpe scale method to the upper 400 m.

A critical step to a successful validation of the latter method resides in the minimization of the effects of instrument noise and measurement errors, which may be due to the conductivity cell's thermal lag, pressure reversals due to ship roll, and salinity spiking caused by the differing time responses of the temperature and conductivity sensors (e.g. Gargett and Garner, 2008). A series of procedures for processing CTD data are given below.

1) For minimizing thermal lag arising from the conductivity cell thermal mass effects, the raw CTD data have been first processed using the Sea-Bird processing software (http://www.seabird.com/pdf_documents/manuals/SBEDataProcessing_7.23.1.pdf). The data processing module "Cell Thermal Mass" performs conductivity thermal mass correction, for which we used typical values (α = 0.03; $1/\beta$ = 7.0) recommended for SBE 9*plus* in the above software.

2) Salinity spiking, which can be caused by misalignment of temperature and conductivity with each other, was removed on acquisition from a pre-programmed SBE 9*plus* deck unit by advancing conductivity by 0.073 seconds. Therefore, there was no need to run the data processing module "Align CTD".

3) Due to the effect of the ship heave motion on the hard-coupled CTD, the fall speed of CTD continuously varies while scanning and can occasionally reverse sign for short periods. We located segments of pressure reversals and edited out the data between successive encounters of the same pressure, although such can be also done via the data processing module "Loop Edit".

4) At this stage, the CTD conductivity and salinity data were corrected with water bottle salinity previously analyzed using a salinometer.

5) In order to further minimize any spike-like anomalies in property (salinity, potential temperature, potential density) profiles, we applied a quadratic fit to successive 10-m segments to detect and discard "extremely abnormal" anomalies surpassing 4 times the root mean square (rms) anomaly relative to the fitting curve. About 0.03% of total scans are eliminated by this process.

6) Our final CTD data processing consisted of averaging and subsampling profiles at regular depth intervals. For this, we averaged the property profiles over a 10-cm window that is centered at each depth incremented by a regular span of 10 cm. On average, about 2 to 3 scans enter into this 10-cm averaging, which is roughly consistent with a mean fall rate of ~0.9 m s^{-1} of our 24 Hz CTD. This filters out any high-frequency random noise of a length scale less than 10 cm, thus the smallest detectable overturn should be of 20 cm in vertical extent. Note also that most density profiles start from 20 m below the sea surface because the near-surface measurements are often found to be much contaminated probably by turbulence generated by the hull. These processed density profiles form our basic data set used in the following section.

3. Thorpe scale analysis

3.1. Thorpe scale and vertical diffusivity

A first step for detecting overturns generated by turbulence in a stratified water column consists of sorting a potential density profile $\rho(z)$, which may contain inversions, into a stable monotonic sequence without inversions. The vertical displacement necessary for generating the stable profile is the Thorpe displacement d, and the Thorpe scale L_T is defined as the rms of d within each overturn that is a region over which the sum of d drops back to zero (Dillon, 1982).

A classical measure of the overturning length is the Ozmidov scale L_O (Ozmidov, 1965) defined as

$$\varepsilon = L_O^2 N^3. \quad (3)$$

Dillon (1982) suggested a linear relationship between L_T and L_O, such that

$$L_O = 0.8\ (\pm\ 0.4)\ L_T, \quad (4)$$

although an exact linear relation between these two overturning scales cannot be expected due to spatial and temporal variability of the turbulent field (Ferron et al., 1998).

Inserting (3) and (4) into (1) and (2), the vertical diffusivity can be estimated indirectly from L_T as

$$K = 0.128\ L_T^2 N, \quad (5)$$

according to the Osborn parameterization, and as

$$K = 1.6 \nu^{1/2} L_T N^{1/2}, \quad (6)$$

according to the Shih parameterization. We give below a series of procedures necessary for an optimal estimation of L_T, thus of K from the Thorpe scale method.

3.2 Determination of a threshold noise level of density

The major concern in the overturn validation is whether the identified overturns are false overturns associated with random noise and/or residual effects of salinity spiking. To prevent false overturns due to random noise, we followed an intermediate density profile method proposed by Gargett and Garner (2008) who modified a profile processing method of Ferron et

al. (1998). The Gargett and Garner method tracks only significant differences in the density profile, where a significant difference is defined relative to a threshold noise level below which a density difference is considered as due to random noise. For this purpose, we have calculated the rms of detrended density anomalies over successive 10-m segments for selected "well-mixed" layers within the cruise data set. This yielded a mean value of 1.75×10^{-4} kg m^{-3}. We considered a multiple of 4 of the latter value, 7×10^{-4} kg m^{-3}, as our threshold noise level. Note that the latter value is close to 5×10^{-4} kg m^{-3} of Gargett and Garner (2008) who applied instead a multiple of 5 to a slightly smaller mean rms density anomaly of 1.0×10^{-4} kg m^{-3} obtained in the Ross Sea region using a SBE 9*plus* CTD.

3.3 Creation of an intermediate density profile

Once the threshold value is determined as above, building an intermediate density profile is straightforward as clearly explained in Gargett and Garner (2008). In short, an intermediate profile is created first from the top to the bottom, maintaining a constant density until a density change greater than the threshold value. A similar profile starting from the bottom to the top is also created and a finale intermediate profile used here is the average of the two individual (downward and upward) profiles. An example of this procedure for determining an intermediate density profile is shown in Fig. 2.

3.4 Validation of overturns

Gargett and Garner (2008) reviewed several previous methods of overturn validation and proposed a practical method using an overturn ratio, $R_o = \min (L^+/L, L^-/L)$, where L is the total vertical extent of an overturn and L^+ (L^-) is the cumulative extent occupied by positive (negative) Thorpe displacements. These authors found the *T*-*S* tightness method suggested by Galbraith and Kelly (1996) unsatisfactory and did not recommend any further rejection based on any measure

of *T*-*S* tightness. Gargett and Garner (2008) reasoned that a single perfect overturn sampled straight through the middle would contain equal lengths (extents) of positive and negative displacements (or R_o = 0.5), and suggested a critical R_o value of 0.2, below which the prospect overturn is suspected of being caused by residual salinity spiking.

We found that the R_o = 0.2 criterion is not sufficient in our case, but the use of R_o = 0.25 at least is rather necessary to detect the false overturns associated with suspicious salinity spiking. An example is given in Fig. 3 for station A3-1, where we observe four clear density spikes as indicated by red arrows. The overturns associated with first two spikes near 200 and 225 m have R_o values between 0.2 and 0.25 (Fig. 3c), thus can be considered as false overturns according to the (R_o =) 0.25 criterion, whereas the 0.2 criterion might have validated them as true overturns. The third spike just above 300 m has a R_o value much smaller than 0.2, thus can be easily discriminated as a false overturn even by the more stringent 0.2 criterion. The fourth spike just below 300 m reveals a R_o value so close to 0.25 that the 0.25 criterion appears to be absolutely necessary for invalidating the prospect overturn. In summary, all four suspected overturns can be safely discriminated as false overturns by our new criterion R_o = 0.25, whereas the previously proposed R_o = 0.2 criterion by Gargett and Garner (2008) fails to detect these false overturns, except for the one associated with the third spike just above 300 m. We will show below that these four suspicious overturns really correspond to false overturns.

3.5 Sensitivity of the vertical diffusivity to its parameterization

With the Thorpe scales L_T obtained based on the R_o = 0.25 criterion, we have calculated vertical diffusivities from the Osborn parameterization (Eq. 5) and the Shih parameterization (Eq. 6), denoted hereafter as K_{O_T} and K_{S_T}, respectively. The regions where no overturns are detected do not necessarily mean no vertical mixing, as already remarked by Ferron et al. (1998), but our method cannot resolve tiny overturns smaller than 20 cm, as mentioned in section 2. In

this case the corresponding diffusivities are set to 1 x 10^{-5} m^2 s^{-1}, a value corresponding to the minimum value (1.024 x 10^{-5} m^2 s^{-1}) of the TurboMAP-derived diffusivities estimated using the Shih parameterization. The resulting diffusivities have been averaged over regular vertical intervals of 10 m. These Thorpe scale-derived diffusivities at station A3-1 are compared in Fig. 4 with those calculated according to (1) and (2) using the TurboMAP-derived ε, denoted hereafter as K_{O_E} and K_{S_E}, respectively (Fig. 4c). We also show in the same figure K_{O_T} and K_{S_T} estimated using the R_o = 0.2 criterion, always in comparison with K_{O_E} and K_{S_E} (Fig. 4b). Several interesting features appear. First, the Thorpe scale-derived diffusivities for the case of R_o = 0.2 are systematically overestimated compared to the TurboMAP-derived diffusivities by up to one to two orders of magnitude in the layer below 80 m, while the converse is true above it in the surface mixed layer. Second, such an overestimation or underestimation in the Thorpe scale-derived diffusivities is much more pronounced by an order of magnitude with the Osborn parameterization (K_{O_T}) compared to the Shih parameterization (K_{S_T}). Third, the TurboMAP-derived diffusivities from both parameterizations (K_{O_E} and K_{S_E}) agree with each other within a factor of 2, on average, except for the surface mixed layer where the difference reaches up to an order of magnitude. As compared to K_{S_E}, there appears to be a tendency of great overestimation (slight underestimation) of K_{O_E} in the surface mixed layer (deeper layer below 80 m). Finally, we observe the efficiency of our new overturn validation criterion, R_o = 0.25 (see Fig. 4c), which yields a much closer agreement with different estimates at the above-mentioned four suspicious false overturns, while the R_o = 0.2 criterion (see Fig. 4b) still yields there abnormal overestimation in the Thorpe scale-derived diffusivities (as compared to microstructure diffusivities). This confirms our previous conviction that the four suspected overturns represent really false overturns which escape from detection with R_o = 0.2 but can be safely detected with R_o = 0.25. We have verified similar features in several other stations too, and we will use hereafter uniquely the R_o = 0.25 criterion for the detection of false overturns.

In order to statistically evaluate the sensitivity of the vertical diffusivity to its parameterization, we have calculated for all intercomparison stations and depths the ratio of the Thorpe scale-derived diffusivities and the TurboMAP-derived diffusivities, separately using the Osborn parameterization (K_{O_T}/K_{O_E}) and the Shih parameterization (K_{S_T}/K_{S_E}) (Fig. 5). There is a clear tendency of overestimation by the Osborn parameterization especially in the layer deeper than 100 m by up to two orders of magnitude or more (Fig. 5a). Such is much less evident with the Shih parameterization which shows a comparatively much compact variability of ratio within an order of magnitude around unity (Fig. 5b). On the other hand, in the surface layer above 100 m there is an increasing negative tendency toward the surface for both parameterizations, as already mentioned. This is probably due to a very low stratification of the surface mixed layer, which prevents detection of moderate overturns whose density differences are smaller than our threshold noise level of 7×10^{-4} kg m^{-3}.

Assuming a log-normal distribution of diffusivity ratios R_{dif}, the mean and standard deviation (std) of log (R_{dif}) have been used for representing the basic statistics of R_{dif}. With the Osborn parameterization (Fig. 5c), the Thorpe scale-derived diffusivities below 200 m overestimate (compared to the TurboMAP-derived diffusivities) by a mean R_{dif} of ~4, with a (±1 std) variability range of (0.7, 20), on average. The overestimation gradually diminishes toward the surface and changes its sign near 80 m to show a near surface peak of underestimation, with a mean R_{dif} of ~0.2 (0.01, 5). In contrast to this, the Shih parameterization (Fig. 5d) yields a much more reasonable agreement, with a mean R_{dif} close to unity (0.3, 3) over most of the water column, except for the surface layer showing always a general but somewhat reduced tendency of underestimation by ~0.4 (0.1, 2). Consequently, we conclude that the use of the Shih parameterization, rather than the Osborn parameterization, is highly desirable in the estimation of vertical diffusivities for our study area, which is also worthy of testing its broad applicability in the other sectors of the Southern Ocean.

4. Thorpe scale-derived vertical diffusivities in the KEOPS2 area

For all KEOPS2 density profiles, we have estimated the Thorpe scale-derived vertical diffusivities K by applying the overturn ration criterion R_o = 0.25 and the Shih parameterization. Figures 6a and 6b represent the spatial distribution of K in the upper 400 m along the approximately north-south (N-S) and east-west (E-W) oriented transects, respectively (see Fig. 1 for the position of stations). The 50-m depth-averaged K values are given in Table 1. Care is warranted to cite the values for the top 50-m depth range because of the above-mentioned underestimation tendency; a multiplication by 2 to 3 is rather recommended. The K distribution is highly heterogeneous in both the vertical and horizontal directions, varying from a low level of $<2 \times 10^{-5}$ m^2 s^{-1} (areas with no color shading) mostly in the Winter Water and the layer below to a relatively high level of $>10^{-4}$ m^2 s^{-1} (areas encircled by white lines) observed predominantly in the upper 150 m. The area-averaged mixing rate in the subsurface layer (200-400 m) over the entire KEOPS2 area is 4×10^{-5} m^2 s^{-1}, a value close to recent estimates from microstructure measurements in a similar layer (250-500 m) north of the Kerguelen Plateau by Waterman et al. (2013). It is also of the same order of magnitude as strain-derived diffusivities from Argo float profiles in the same area (Whalen et al., 2012; Wu et al., 2011). For comparison, somewhat contrasting results have been reported in the PF region of Drake Passage; elevated subsurface diffusivities of $O(10^{-4})$ m^2 s^{-1} have been estimated from Thorpe scales and CTD strain by Thompson et al. (2007), whereas direct microstructure measurements of turbulence levels by St. Laurent et al. (2012) have rather revealed a much weaker background level of $O(10^{-5})$ m^2 s^{-1} (see also Waterhouse et al., 2014), similar to the estimates in the Kerguelen region.

The spatial K distribution appears to have some correlation with the regional frontal circulation carrying different water masses. For example, in the N-S transect (Fig. 6a) the areas of elevated diffusivities are mostly confined in the seasonal thermocline (50-150 m) above the

Winter Water (Tmin < 2°C) developed to the south of the PF, with the exception over the continental slope east of the Kerguelen Islands (TNS 7 to 9) where the mixing rate is low. The strongest diffusivities are found over the shallow plateau (~600 m) southeast of the islands (TNS 10 and A3-1) and close to the PF over the northern escarpment northeast of the islands (TNS 3 to 5). Our results are consistent with similar previous results showing enhanced turbulent levels in the regions where deep reaching strong flow meets a rugged or abrupt bottom topography (Wu et al., 2011; St Laurent et al., 2012; Whalen et al., 2012; Waterman et al., 2013; Waterhouse et al., 2014). Note that most of these stations of elevated diffusivities are associated with a local patch of high chlorophyll or its downstream extension, with the exception at TNS 5 where a local minimum in chlorophyll is observed instead (see Fig. 1b), for unknown reasons. On the other hand, the Winter Water layer (150-250 m) generally coincides with the layer of diffusivity minimum. Also, the mixing rate in warmer waters north of the PF (TNS 1 to 2) is quite low throughout the upper 400 m, resting close to its background level of $O(10^{-5})$ m^2 s^{-1}.

The diffusivity estimates at A3-1 are similar in vertical structure but smaller in magnitude by a factor of 4 than those estimated at the same station during the 2005 KEOPS1 cruise (Park et al., 2008). Several factors may explain this difference. First, in Park et al. (2008) the discrimination of false from true overturns was based on the criterion that a minimum density difference of 0.0015 kg m^{-3} (or three times the estimated noise level of 0.0005 kg m^{-3}) is necessary to validate an overturn. As will be seen later in the discussion section, such a density difference criterion is inefficient to discriminate the false overturns associated with density spikes. Therefore, the latter criterion tends to overestimate the mixing rates as compared to the overturn ratio criterion which is found to be agreeably efficient especially with R_o = 0.25 (see Figs. 3, 4). Second, Park et al. (2008) used the Osborn parameterization which is found to yield mean diffusivities significantly higher by a factor of 4 compared to the Shih parameterization adapted in the present study (see Fig. 5).

On the E-W transect (Fig. 6b), the spatial distribution of K is quite complex compared to the N-S section and there does not appear any simple pattern that can be easily connected to the frontal circulation of water masses. Nevertheless, we remark a relatively strong mixing rate of $O(10^{-4})$ m^2 s^{-1} over much of the water column at E1-4W that is located close to the northward flowing PF along the escarpment east of the Kerguelen Islands, while the weakest rate of $O(10^{-5})$ m^2 s^{-1} is observed at TEW7 where warmer polar frontal zone waters flow southward (Park et al., 2014) along with the southward retroflecting PF (see also Fig. 1b). Other stations on the section show a highly undulating vertical structure with a moderate mixing rate less than 5 x 10^{-5} m^2 s^{-1}, in general.

5. Discussion and Conclusions

5.1 Comparison with a displacement shape method

Recently, van Haren and Gostiaux (2014) suggested a new method of discriminating various overturns and intrusions via inspection of displacement (d) shapes in a d-z plane. They showed that depending on the displacement slopes z/d, the true overturns can be categorized into different types of vortex, such as most frequent half-turn Rankine votices (½ < z/d < 1) and rather rare full-turn Rankine votices (z/d ~ 1) or solid-body rotations (z/d = ½). These authors recommended to use temperature profiles rather than density profiles if salinity-compensating intrusions are negligible, because the density profiles are much noisier thus cause an overestimate of turbulence parameters. They mentioned also that more or less equivalent results (within a factor of 1.5) may be obtained with the density data only by imposing a limit of discarding density variations smaller than 1 x 10^{-3} kg m^{-3}, twice the expected noise level.

In our case of the upper layer of the Antarctic zone the temperature is not an adequate parameter for investigating overturns because of its unstable vertical distribution, with a gradual temperature increase with depth from the Winter Water (Tmin < 2°C) centered at about 200 m to

the Upper Circumpolar Deep Water (Tmax ~ 2.3°C) centered at about 700 m (Park et al., 2014). Then, we have tested the method using corrected density profiles after discarding density variations (relative to sorted density profiles) smaller than the proposed limit of 1 x 10^{-3} kg m^{-3} by van Haren and Gostiaux, (2014).

An example of the test is given in Fig. 7 for station A3-1 already discussed in Figs. 3 and 4 and where there exist four clear density spikes (red arrows). van Haren and Gostiaux (2014) previously remarked that discarding density variations <1 x 10^{-3} kg m^{-3} unfortunately limits the use of investigating the shape of displacements. Consistent with this remark, discriminating various types of overturns by inspection of displacement shapes does not appear very obvious (Fig. 7b). Nevertheless, we observe that the most significant displacements appear mostly in the vicinity of the above four density spikes, with a rather marked asymmetry between positive and negative displacements. As before, the mixing rates have been estimated using the Shih parameterization (Eq. 6) and the Thorpe scales L_T of identified overturns. The red line in Fig. 7c illustrates the resultant diffusivities averaged over intervals of 10 m, in comparison with those from our best approach of the Thorpe scale method (using intermediate density profiles and applying the overturn ratio criterion R_o = 0.25 and the Shih parameterization: black line) and the TurboMAP measurements (blue line). Note that the latter two lines are borrowed from Fig. 4c. Compared to our best approach and the TurboMAP data, the displacement shape method yields in many places comparable diffusivities within a factor of 2, but with a great exception in the vicinity of the above four density spikes where we observe a significant overestimation (relative to the TurboMAP data) by as much as an order of magnitude. This indicates that in great contrast to our approach, the displacement shape method does not able to discriminate the false overturns associated with apparent density spikes (caused probably by a mismatch between the temperature and conductivity sensors), the major cause of most false overturns in the oceans (e.g., Galbraith and Kelley, 1996; Gargett and Garner, 2008).

5.2 Concluding remarks

We have validated the Thorpe scale-derived vertical diffusivities in the PF region east of the Kerguelen Islands using more direct estimates from the TurboMAP microprofiler measurements at selected stations during the KEOPS2 cruise. We have emphasized the need of a careful treatment of raw CTD data to obtain density profiles as fine as possible but with a maximum removal of random noise and measurement errors. Here we have used density profiles of 10 cm scales, which can yield fine resolution diffusivities at scales up to 10 m after a suitable vertical averaging. This vertical resolution is far finer by an order of magnitude compared to other indirect strain and shear methods that use a vertical integration scale of the order of 200 m (e.g., Thompson et al., 2007; Frants et al., 2013). A compelling argument for obtaining such finely resolved diffusivities from the Thorpe scale method may be that they should provide, as compared to coarser estimates from the strain and shear methods, detailed local information useful for precisely evaluating the vertical fluxes of nutrients and other biogeochemical materials across the seasonal thermocline.

Our comparative results are found to be sensitive to the choice of the parameterization of diffusivity and the overturn validation criteria. The use of the Shih parameterization (Eqs. 2 and 6) combined with our overturn ratio criterion of R_o = 0.25 has yielded significantly better results by a factor of 5 compared to the results from the Osborn parameterization (Eqs. 1 and 5) and the R_o = 0.2 criterion suggested by Gargett and Garner (2008). The latter criterion (R_o = 0.2) appears to be insufficient (too low) to detect most false overturns associated with apparent density spikes, thus overestimating diffusivities. Moreover, the Osborn parameterization is shown to be much more sensitive to such an overestimation compared to the Shih parameterization. This study demonstrates that the Thorpe scale method remains as a useful tool for investigating the fine scale diffusivities in the Southern Ocean if one makes judicious use of the combined Shih parameterization and R_o = 0.25 criterion. This is in stark contrast to Frants et al. (2013) who

claimed the real limitations of the CTD-based fine structure methods in Drake Passage and the eastern Pacific sector of the Southern Ocean.

The Thorpe scale-derived vertical diffusivities in the KEOPS2 region vary from a background level of $O(10^{-5})$ m^2 s^{-1} in the Winter Water layer to a relatively high level of $O(10^{-4})$ m^2 s^{-1} in the seasonal thermocline which is a transitional boundary layer between the Winter Water and the surface mixed layer. The latter high diffusivity feature is especially pronounced at stations over the shallow plateau southeast of the Kerguelen Islands and in the cold side of the PF running along the escarpment northeast of the islands. This is consistent with the general belief that the interaction of strong flow with rough or abrupt bottom topography produces high internal wave energy and intensified turbulence (e.g., Ferron et al., 1998; Klymak et al., 2008; St Laurent et al., 2012; Waterman et al., 2013). On the other hand, at stations immediately north of the PF where warmer surface waters are encountered, diffusivity values are particularly low.

Aknowledgements

We thank the IPEV for financial and logistical support and the captain and crew of the R/V *Marion Dufresne* for their professional contributions to various field experiments during the 2011 KEOPS2 cruise. We are also grateful to S. Blain, project manager, and B. Queguiner, chief scientist, for their great effort for making the KEOPS2 cruise successful. We thank two anonymous reviewers for constructive comments which have significantly improved the original manuscript. All co-authors of the present paper have benefited by the STAR program, a French-Korean research collaboration program, for their mutual exchanges in 2012 and 2013. JHL was partially supported by the National Research Foundation of Korea Grant funded by the Korean Government (NRF-2009-C1AAA001-0093065) to participate in the KEOPS2 cruise.

References

433 Dillon, T. M.: Vertical overturns: A comparison of Thorpe and Ozmidov length scales. J.
434 Geophys. Res., 87, 9601-9613, 1982.
435 Ferron, B., H. Mercier, K. Speer, A. Gargett and K. Polzin: Mixing in the Romanche fracture
436 zone. J. Phys. Oceanogr., 28, 1929-1945, 1998.
437 Frants, M., G. M. Damerell, S. T. Gille, K. J. Heywood, J. MacKinnon and J. Springtall: An
438 assessment of density-based fines-cale methods for estimating diapycnal diffusivity in the
439 Southern Ocean, J. Atmos. Oceanic Technol., 30, 2647-2661, doi: 10.1175/jtech-d-12-
440 00241.1, 2013.
441 Galbraith, P. S. and D. E. Kelley: Identifying overturns in CTD profiles. J. Atmos. Oceanic
442 Technol., 13, 688-702, 1996.
443 Gargett, A. and T. Garner: Determining Thorpe scales from ship-lowered CTD density profiles. J.
444 Atmos. Oceanic Technol., 25, 1657-1670, doi:10.1175/2008JTECHO541.1, 2008.
445 Klymak, J. M., R. Pinkel and L. Rainville: Direct breaking of the internal tide near topography:
446 Kaena Ridge, Hawaii. J. Phys. Oceanogr., 38, 380-399, doi:10.1175/2007JPO3728.1,
447 2008.
448 Osborn, T. R.: Estimates of the local rate of vertical diffusion from dissipation measurements. J.
449 Phys. Oceanogr., 10, 83-89, 1980.
450 Ozmidov, R. V.: On the turbulent exchange in a stably stratified ocean. Izv. Acad. Sci., USSR
451 Atmos. Oceanic Phys., 1, 853-860, 1965.
452 Park, Y.-H., J. L. Fuda, I. Durand and A. C. Naveira Garabato: Internal tides and vertical mixing
453 over the Kerguelen Plateau. Deep-Sea Res. II, 55, 582-593, 2008.
454 Park, Y.-H., I. Durand, E. Kestenare, G. Rougier, M. Zhou, F. d'Ovidio, C. Cotté and J.-H. Lee:
455 Polar Front around the Kerguelen Islands: An up-to-date determination and associated
456 circulation of surface/subsurface waters. J. Geophys. Res. Ocean, 119,
457 doi:10.1002/2014JC010061, 2014.

458 Shih, L. H., J. R. Koseff, G. N. Ivey and J. H. Ferziger: Parameterization of turbulent fluxes and
459 scales using homogeneous sheared stably stratified turbulence simulations. J. Fluid Mech.,
460 525, 193-214, 2005.
461 St. Laurent, L. C., A. C. Naveira Garabato, J. R. Ledwell, A. M. Thurnherr, J. M. Toole, and A. J.
462 Watson: Turbulence and diapycnal mixing in Drake Passage. J. Phys. Oceanogr., 42,
463 2143–2152, doi:10.1175/JPO-D-12-027.1, 2012.
464 Thompson, A. F., S. T. Gille, J. A. MacKinnon, and J. Sprintall: Spatial and temporal patterns of
465 small-scale mixing in Drake Passage. J. Phys. Oceanogr., 37, 572–592,
466 doi:10.1175/JPO3021.1, 2007.
467 Thorpe, S. A.: Turbulence and mixing in a Scottish Loch. Philos. Trans. Roy. Soc. London,
468 286A, 125-181, 1977.
469 van Haren, H. and L. Gostiaux: Characterizing turbulent overturns in CTD-data. Dyn. Atmos.
470 Ocean, 66, 58-76, 2014.
471 Waterhouse A. F., J. A. MacKinnon, J. D. Nash, M. H. Alford, E. Kunze, H. L. Simmons, K. L.
472 Polzin, L. C. St. Laurent, O. M. Sun, R. Pinkel, L. D. Talley, C. B. Whalen, T. N. Hussen,
473 G. S. Carter, I. Fer, S. Waterman, A. C. Naveira Garabato, T. B. Sanford, and C. M. Lee:
474 Global pattern of diapycnal mixing from measurements of the turbulent dissipation rate. J.
475 Phys. Oceanogr., 44, 1854-1872, doi :10.1175/JPO-D-13-0104.1, 2014.
476 Waterman, S., A. C. Naveira Garabato, and K. L. Polzin: Internal waves and turbulence in the
477 Antarctic Circumpolar Current. J. Phys. Oceanogr., 43, 259–282, doi:10.1175/JPO-D-11-
478 0194.1, 2013.
479 Whalen, C., L. D. Talley, and J. A. MacKinnon: Spatial and temporal variability of global ocean
480 mixing inferred from Argo profiles. Geophys. Res. Lett., 39, L18612, doi:10.1029/
481 2012GL053196, 2012.

Wu, L. X., Z. Jing, S. Riser, and M. Visbeck: Seasonal and spatial variations of Southern Ocean diapycnal mixing from Argo profiling floats, Nat. Geosci., 4, 363–366, doi:10.1038/ngeo1156, 2011.

Table 1. 50-m averaged vertical diffusivities (in 10^{-5} m^2 s^{-1}) at A3-1 estimated from the Thorpe scale method using the Shih parameterization and the R_o = 0.25 criterion.

Station	depth range (m)							
	0-50	50-100	100-150	150-200	200-250	250-300	300-350	350-400
TNS10	44	37	34	2	6	1	5	2
TNS09	22	5	1	4	2	1	6	19
TNS08	18	8	1	8	1	3	6	7
TNS07	2	2	1	1	2	2	12	5
TNS06	34	11	7	4	2	6	3	2
TNS05	16	18	13	1	9	9	5	2
TNS04	67	19	5	1	1	11	1	2
TNS03	16	22	27	2	2	3	6	1
TNS02	1	1	1	1	1	5	1	1
TNS01	1	4	3	1	1	3	1	1
TEW01	20	4	NaN	NaN	NaN	NaN	NaN	NaN
TEW02	1	1	NaN	NaN	NaN	NaN	NaN	NaN
TEW03	1	4	2	3	1	21	2	1
TEW04	1	2	5	4	2	2	7	2
TEW05	1	6	1	3	2	8	4	4
TEW06	1	2	7	1	2	4	1	5
TEW07	1	1	7	1	1	2	3	2
TEW08	2	4	1	2	2	11	7	9
A3-1	13	18	13	2	1	1	2	5
E1-2	4	1	3	6	1	2	6	2
E1-4W	9	19	24	14	19	7	1	9
NPF-L	6	5	6	18	2	3	6	3

Figures captions

Fig. 1. (a) Map showing the KEOPS2 CTD stations (red dots) on or close to two N-S and E-W transects superimposed on the detailed bathymetry. The concomitant TurboMAP microstructure profiler stations are indicated by blue circles. Isobaths greater than 500 m are given every 500 m and the seabed shallower than 200 m (100 m) is lightly (darkly) shaded. (b) These stations are also superimposed on a representative satellite image of chlorophyll concentration (colors) and a surface geostrophic velocity field (arrows) constructed from the combined data sets from altimetry and trajectories of drifters launched during the cruise. The geographical position of the Polar Front (PF) is indicated. This figure (b) has been adapted from Park et al. (2014).

Fig.2. Sample section of intermediate profiles generated from the top (red), from the bottom (blue), and from the average of these two (thick black) of a measured density profile (thin black), following the method of Gargett and Garner (2008). The threshold density noise (0.0007 kg m^{-3}) used is indicated.

Fig.3. Sample illustration showing the (a) intermediate density profile, (b) Thorpe scales, and (c) overturn ratios calculated at A3-1. Four suspicious false overturns associated with abnormal spikes clearly apparent in the density profile are indicated by red arrows. Two criteria of overturn validation are shown by coloured vertical lines in (c): blue for R_o = 0.2 and red for R_o = 0.25.

Fig.4. Different diffusivity profiles at A3-1 calculated with different pairs of parameterization (Osborn or Shih) and observational method (Thorpe scale L_T or TurboMAP-derived ε) using the two overturn validation criteria of (b) R_o = 0.2 and (c) R_o = 0.25. Note that the four abnormal

545 spikes seen in (a), which being the repetition of Fig. 3a, give rise to great overestimation in the
546 Thorpe scale-derived diffusivities with R_o = 0.2, but such a feature disappears completely with
547 R_o = 0.25.
548
549 Fig.5. Ratio profiles of the Thorpe scale-derived diffusivities and the TurboMAP-derived
550 diffusivities at all intercomparison stations based on (a) the Osborn parameterization and (b) the
551 Shih parameterization. Here, the R_o = 0.25 criterion is commonly used. (c) and (d) are same as (a)
552 and (b) but for the mean (black) and standard deviation (grey) of all stations.
553
554 Fig.6. Thorpe scale-derived diffusivity sections (calculated using the Shih parameterization and
555 the R_o = 0.25 criterion) of the upper 400 m on (a) the N-S transect and (b) the E-W transect (top
556 panels; see Fig. 1 for locations of the transects and stations). Diffusivity K values, which range
557 from 1 x 10^{-5} m^2 s^{-1} to 7 x 10^{-4} m^2 s^{-1}, are shown in log (K). White and black lines correspond to
558 1 x K = 10^{-4} m^2 s^{-1} and K = 5 x 10^{-5} m^2 s^{-1}, respectively, while the regions without colour shading
559 to K < 2 x 10^{-5} m^2 s^{-1}. For easy of interpretation in combination with the 3-D frontal circulation
560 of water masses (see also Fig. 1), corresponding temperature sections (middle panels) and seabed
561 profiles drawn from in situ station depths measured during the KEOPS2 cruise (bottom panels)
562 are also shown.
563
564 Fig.7. (a) Potential density profile in the 150-400 m layer at A3-1, with four clear density spikes
565 being indicated by red arrows. (b) Displacement points (red dots) computed from corrected
566 density data after discarding density variations smaller than 1 x 10^{-3} kg m^{-3}. Displacement slopes
567 z/d = 1 (solid) and z/d = 1/2 (dashed) are superimposed. (c) Diffusivity profile estimated from the
568 displacement shape method (red) in comparison with those from our best approach (black) and

TurboMAP data (blue), all using the Shih parameterization. See the text for more details. Red arrows indicate the location of the density spikes seen in (a).

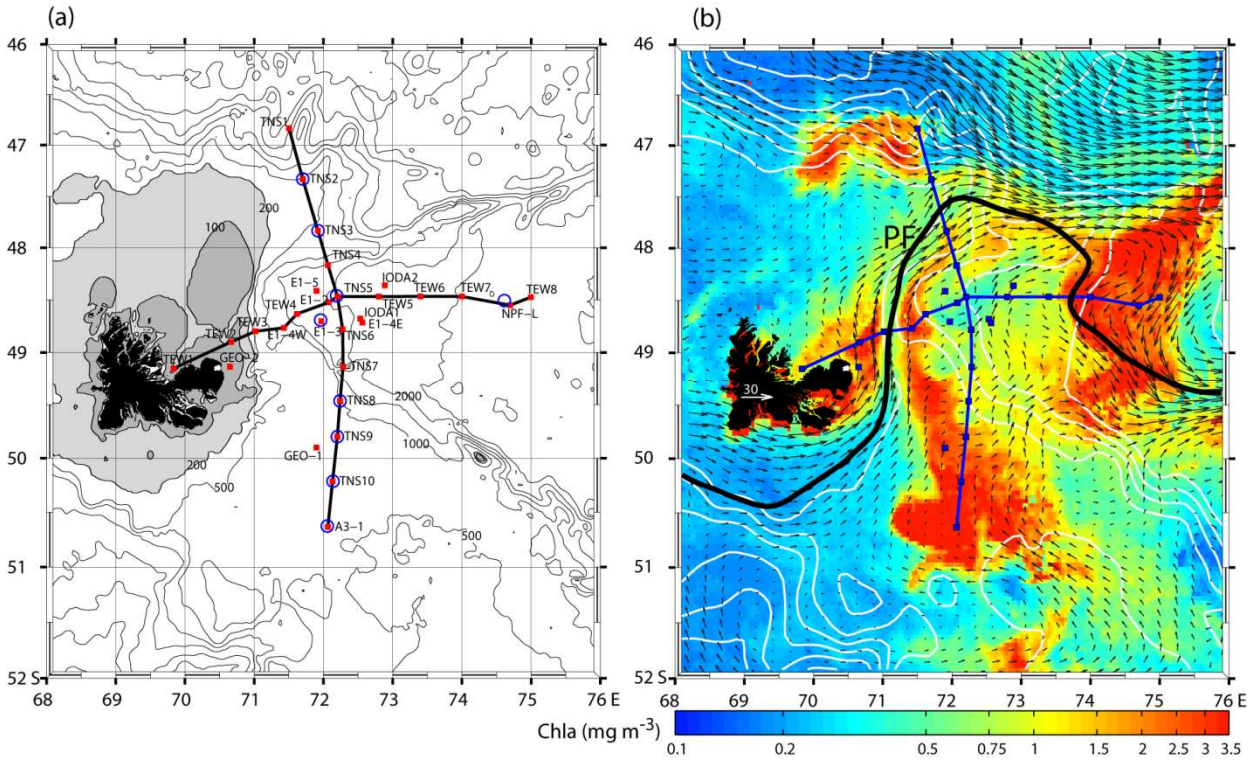

586

587

588 Fig. 1. (a) Map showing the KEOPS2 CTD stations (red dots) on or close to two N-S and E-W
589 transects superimposed on the detailed bathymetry. The concomitant TurboMAP microstructure
590 profiler stations are indicated by blue circles. Isobaths greater than 500 m are given every 500 m
591 and the seabed shallower than 200 m (100 m) is lightly (darkly) shaded. (b) These stations are
592 also superimposed on a representative satellite image of chlorophyll concentration (colors) and a
593 surface geostrophic velocity field (arrows) constructed from the combined data sets from
594 altimetry and trajectories of drifters launched during the cruise. The geographical position of the
595 Polar Front (PF) is indicated. This figure (b) has been adapted from Park et al. (2014).
596
597

598

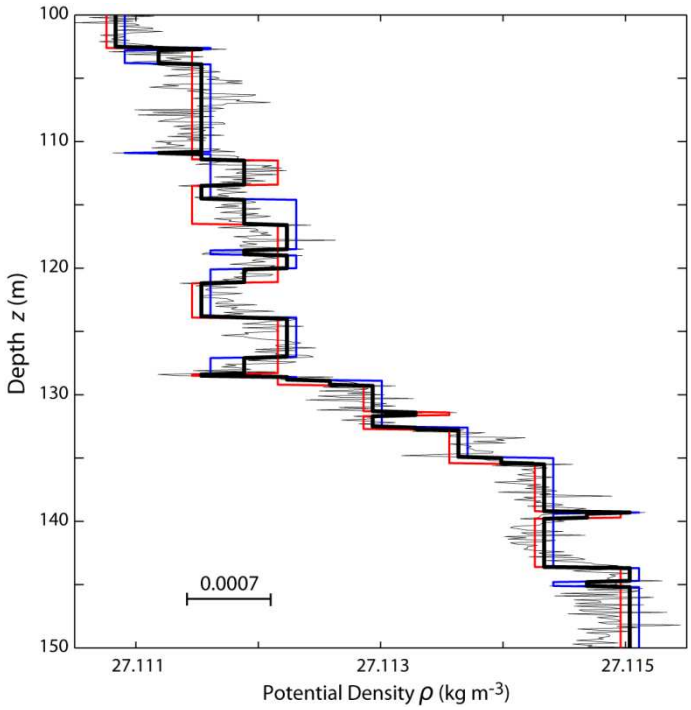

599
600
601 Fig.2. Sample section of intermediate profiles generated from the top (red), from the bottom
602 (blue), and from the average of these two (thick black) of a measured density profile (thin black),
603 following the method of Gargett and Garner (2008). The threshold density noise (0.0007 kg m^{-3})
604 used is indicated.
605
606
607

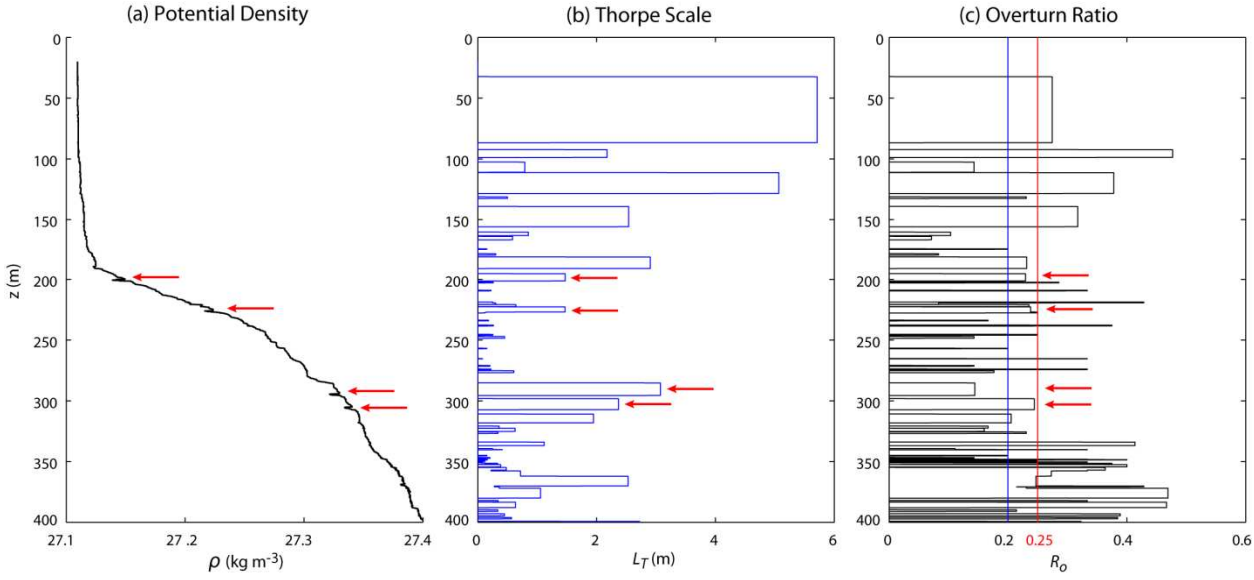

608
609
610 Fig.3. Sample illustration showing the (a) intermediate density profile, (b) Thorpe scales, and (c)
611 overturn ratios calculated at A3-1. Four suspicious false overturns associated with abnormal
612 spikes clearly apparent in the density profile are indicated by red arrows. Two criteria of
613 overturn validation are shown by coloured vertical lines in (c): blue for R_o = 0.2 and red for R_o =
614 0.25.

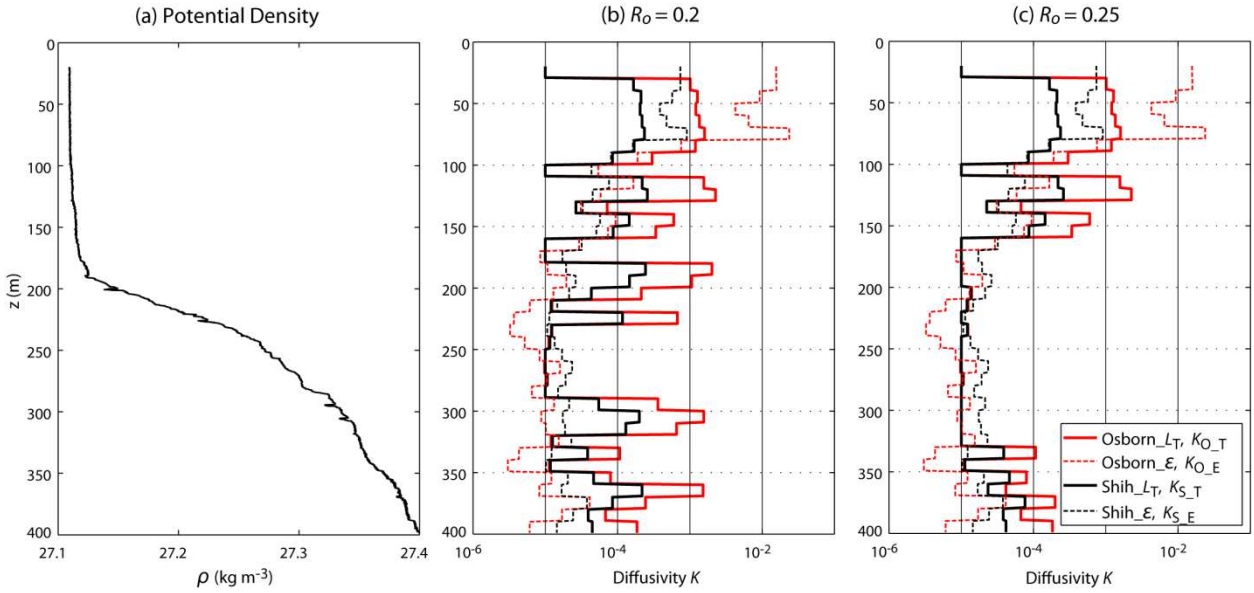

615
616
617 Fig.4. Different diffusivity profiles at A3-1 calculated with different pairs of parameterization
618 (Osborn or Shih) and observational method (Thorpe scale L_T or TurboMAP-derived ε) using the
619 two overturn validation criteria of (b) R_o = 0.2 and (c) R_o = 0.25. Note that the four abnormal
620 spikes seen in (a), which being the repetition of Fig. 3a, give rise to great overestimation in the
621 Thorpe scale-derived diffusivities with R_o = 0.2, but such a feature disappears completely with
622 R_o = 0.25.
623
624
625
626
627

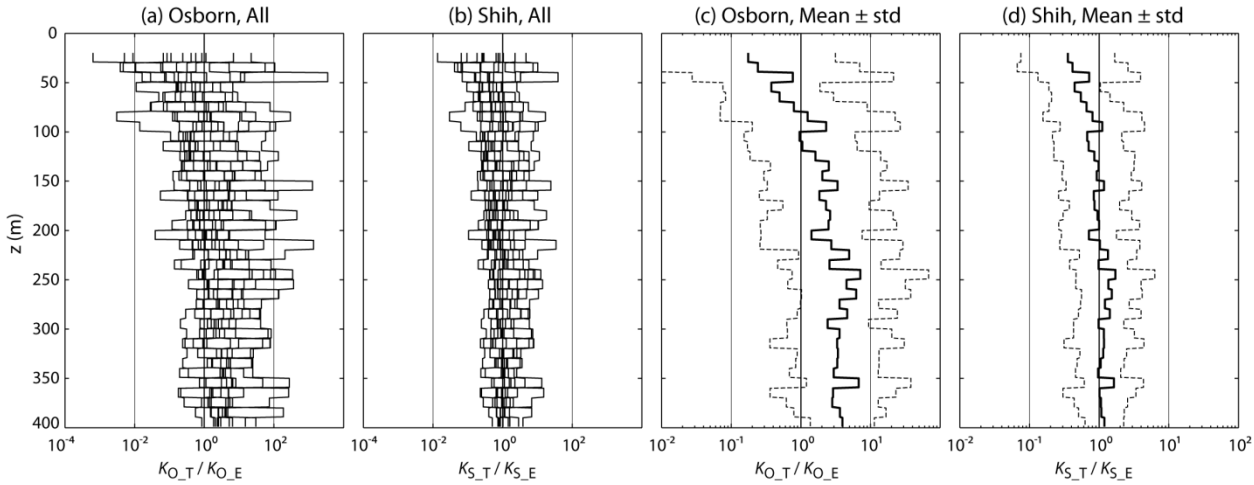

628
629
630 Fig.5. Ratio profiles of the Thorpe scale-derived diffusivities and the TurboMAP-derived
631 diffusivities at all intercomparison stations based on (a) the Osborn parameterization and (b) the
632 Shih parameterization. Here, the R_o = 0.25 criterion is commonly used. (c) and (d) are same as (a)
633 and (b) but for the mean (black) and standard deviation (grey) of all stations.
634
635
636

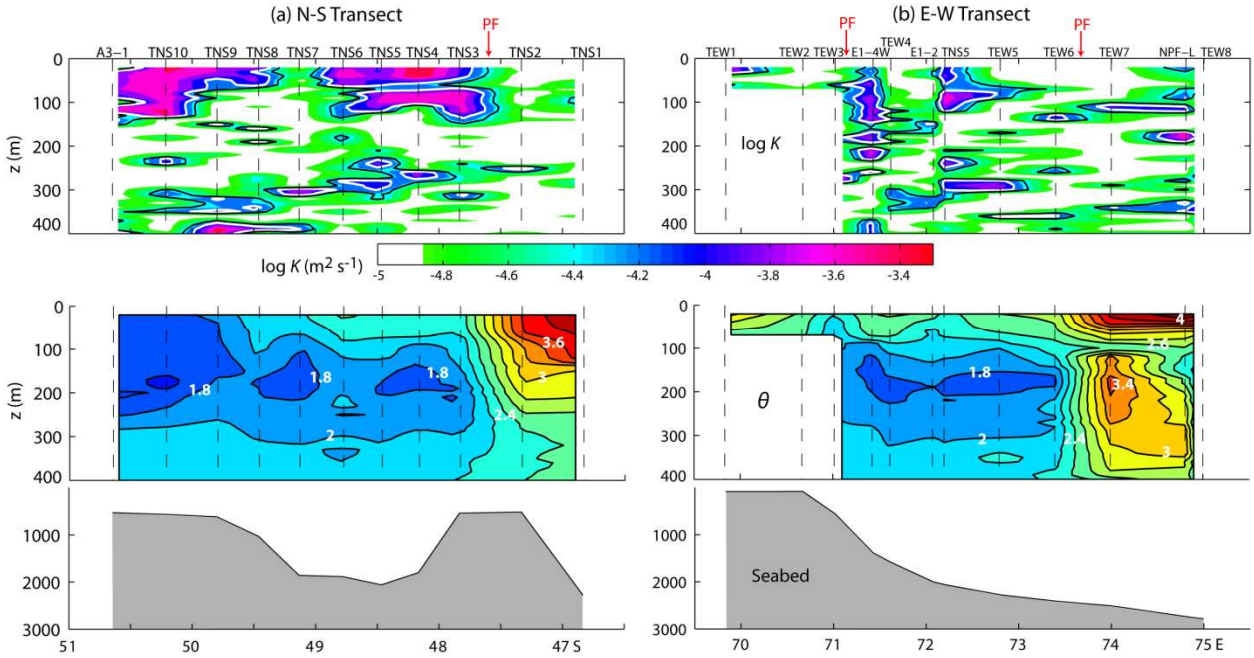

Fig.6. Thorpe scale-derived diffusivity sections (calculated using the Shih parameterization and the R_o = 0.25 criterion) of the upper 400 m on (a) the N-S transect and (b) the E-W transect (top panels; see Fig. 1 for locations of the transects and stations). Diffusivity K values, which range from 1 x 10^{-5} m^2 s^{-1} to 7 x 10^{-4} m^2 s^{-1}, are shown in log (K). White and black lines correspond to K = 1 x 10^{-4} m^2 s^{-1} and K = 5 x 10^{-5} m^2 s^{-1}, respectively, while the regions without colour shading to K < 2 x 10^{-5} m^2 s^{-1}. For easy of interpretation in combination with the 3-D frontal circulation of water masses (see also Fig. 1), corresponding temperature sections (middle panels) and seabed profiles drawn using in situ station depths measured during the KEOPS2 cruise (bottom panels) are also shown.

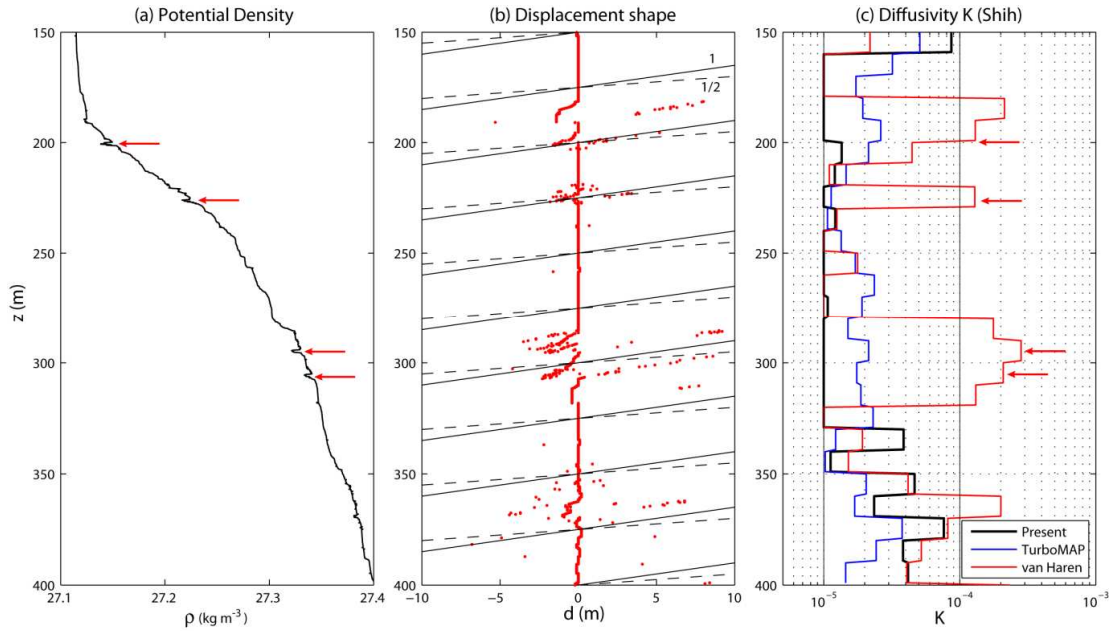

Fig.7. (a) Potential density profile in the 150-400 m layer at A3-1, with four clear density spikes being indicated by red arrows. (b) Displacement points (red dots) computed from corrected density data after discarding density variations smaller than 1 x 10^{-3} kg m^{-3}. Displacement slopes z/d = 1 (solid) and z/d = 1/2 (dashed) are superimposed. (c) Diffusivity profile estimated from the displacement shape method (red) in comparison with those from our best approach (black) and TurboMAP data (blue), all using the Shih parameterization. See the text for more details. Red arrows indicate the location of the density spikes seen in (a).